Journal of Engineering for Gas Turbines and Power. received June 26, 2016;
Accepted manuscript posted August 2, 2016. DOI:10.1115/1.4034020

GTP-16-1081

PREDICTION AND ANALYSIS OF IMPACT OF TBC OXIDATION ON GAS TURBINE CREEP LIFE

E.A. Ogiriki *ebitoski@yahoo.com*
Y.G. Li *i.y.li@cranfield.ac.uk*
Th. Nikolaidis *t.nikolaidis@cranfield.ac.uk*

School of Aerospace, Transport and Manufacturing, Cranfield University, Cranfield, Bedford, MK43 0AL, UK.

ABSTRACT

Thermal Barrier Coatings (TBC) have been widely used in the power generation industry to protect turbine blades from damage in hostile operating environment. This allows either a high Turbine Entry temperature (TET) to be employed or a low percentage of cooling air to be used, both of which will improve the performance and efficiency of gas turbine engines. However, with continuous increases in turbine entry temperature aimed at improving the performance and efficiency of gas turbines, TBCs have become more susceptible to oxidation. Such oxidation has been largely responsible for the premature failure of most TBCs. Nevertheless, existing creep life prediction models that give adequate considerations to the effects of TBC oxidation on creep life are rare. The implication is that the creep life of gas turbines may be estimated more accurately if TBC oxidation is considered. In this paper, a performance-based integrated creep life model has been introduced with the capability of assessing the impact of TBC oxidation on the creep life and performance of gas turbines. The model comprises of a thermal, stress, oxidation, performance, and life estimation

models. High Pressure Turbine (HPT) blades are selected as the life limiting component of gas turbines. Therefore the integrated model was employed to investigate the effect of several operating conditions on the HPT blades of a model gas turbine engine using a Creep Factor approach. The results show that different operating conditions can significantly affect the oxidation rates of TBCs which in turn affect the creep life of HPT blades. For instance, TBC oxidation can speed up the overall life usage of a gas turbine engine from 4.22% to 6.35% within one year operation. It is the objective of this research that the developed method may assist gas turbine users in selecting the best mission profile that will minimize maintenance and operating costs while giving the best engine availability.

INTRODUCTION

The general trend in the gas turbine power generation industry has been towards increasing the firing temperature and the pressure ratios of the engines which are aimed at improving the efficiency and performance of gas turbine engines [1-3]. Thus, pressure ratios up to 40 and TET up to 1700K have been achieved in gas turbine engine designs, with materials being capable of operating at temperatures in excess of 1223K [4]. This increase in firing temperature has required subsequent advanced designs of gas turbine engine components, such as super alloy turbine blades and vanes. To meet these requirements, TBC comprising alumina or zirconia based ceramics, which provide an insulating protection layer, were introduced in the mid-1970s and by early 1980s they had entered revenue service on the vane platforms of aircraft engines [5]. Since inception, TBCs have become a

critical aspect of gas turbines as they have enabled gas turbine engines to operate at significantly higher firing temperatures hence improving their power ratings and thermal efficiencies. However, as TETs are continuously increased in pursuit of better performance and efficiencies, TBCs have become more susceptible to time-dependent damage such as corrosion and oxidation. The situation becomes worse when gas turbines are operated in chemically aggressive environments and harsh operating conditions.

Since TBCs are critical to gas turbine engine operations, their failure has significant impact on gas turbine engine creep life; exposing the blade substrate material to very high temperatures. However, existing creep life models that give adequate consideration to the impact of TBC failure on gas turbine creep life are rare. Most of the existing creep life prediction models only predict the time to failure of the blades without considering the failure of blade coatings. In addition, studies conducted and reported on the effects of TBC failure on gas turbines creep life are from a metallurgical point of view [6]; hence limited information is available in the public domain about the influence of TBC failure on gas turbine creep life from a performance perspective.

TBC failure during operations may be attributed to damage phenomena such as thermal cycling fatigue, erosion, high temperature corrosion, oxidation etc. [7-8]. This paper aims at introducing a performance-based integrated creep life model being capable of predicting the impact of TBC oxidation on gas turbine creep life. An application of the developed model to a model gas turbine engine on TBC damage and HPT blade creep life

prediction at different operating conditions is demonstrated to prove the effectiveness of the model.

METHODOLOGY

A HPT blade of a two-shaft aero derivative model gas turbine engine is selected as the creep life limiting component of the gas turbine. This is due to the fact that it experiences the highest oxidation, mechanical and thermal loads. Consequently, the idea of this research is to analyze the effect of TBC oxidation on the creep behavior of the HPT blade using a Creep Factor approach [9]. In doing this, an engine performance model was created using TURBOMATCH [10], which is a gas turbine performance simulation code developed at Cranfield University. A creep life model was set up and the data from the performance model and information available in open literature was used for the prediction of engine creep life. Thereafter, a TBC oxidation model was developed and incorporated into the creep life model. The integrated model was subsequently used to assess the impact of TBC oxidation on the creep life and performance of the model gas turbine engine.

TBC Oxidation Model

The oxidation model adopted in this research was developed by Meier et al [11]. The model has the capability to predict the failure of both Air-Plasma-Spray (APS) and Electron-Beam Physical-Vapor Deposition (EB-PVD) TBCs. It identifies Thermally Grown Oxide (TGO) and strain rate as the important and critical factors responsible for TBC failure. TGO is critical

because it is largely responsible for Bond Coat (BC) oxidation and thermal mismatch stresses which are largely responsible for the speedy spallation of the top coat (TC) [12-14]. The TGO growth is responsible for the constrained volume expansion which most times leads to the compressive "growth" stresses that persist at all temperatures. Upon cooling, the thermal-expansion mismatch between the TGO and the BC leads to very high thermal compressive residual stresses in the TGO which reach a maximum at T_{amb}. The strain energy in the TGO scales linearly with the TGO thickness and quadratically with the TGO stress, and drives fracture [15-16]. In this model, failure is assumed to have occurred when there is crack initiation. The damage model was taken to be a power law relation shown in Equation (1) [11].

$$\mathrm{N} = \mathrm{A}\Delta\varepsilon^{m} \qquad \textbf{(1)}$$

where N is the number of cycles to failure, A is a coefficient whose value depends on the amount of oxide growth, ϵ is TGO strain and m is an empirical power law coefficient. The TGO growth is presented with Arrhenius behavior as expressed in Equation (2).

$$\delta = \{\exp\left[\mathrm{Q}\left(\frac{1}{T_0} - \frac{1}{T}\right)\right] t\}^{n} \qquad \textbf{(2)}$$

where δ is TGO thickness, t is time, Q represents $\Delta H/R$, where ΔH is change in enthalpy, R is gas constant, T_0 is the temperature at a reference condition, T is gas temperature and n is a constant. The TGO thickness δ in Equation

(2) determines the constant of proportionality and the life is expressed in Equation (3).

$$\mathrm{N} = [\left(\frac{\Delta\varepsilon_{ff}}{\Delta\epsilon}\right)(1-\frac{\delta}{\delta_C})^c + (\frac{\delta}{\delta_C})^c]^b \qquad \textbf{(3)}$$

where $\Delta\epsilon$ is the TGO inelastic strain range, *b* and *c* are model constants, $\Delta\varepsilon_{ff}$ is the mechanical inelastic strain range that causes failure in one cycle, *δ* is the oxide growth per cycle (TGO thickness) calculated in Equation (2) and δ_C is the critical oxide thickness that causes spallation without cycling. The critical thickness, δ_C value is normally taken between 5-6μm [17] and is around 3μm in the case of APS-TBCs [18]. The mechanical strain for a cycle in the TGO is calculated using Equation (4).

$$\varepsilon(\mathrm{T}) = \varepsilon_{SS}(\mathrm{T}) - \frac{\Delta L(T)}{L} \qquad \textbf{(4)}$$

where *ε* is the mechanical strain, ε_{SS} is the substrate total strain and $\frac{\Delta L(T)}{L}$ is the coefficient of thermal expansion (CTE). The coefficient of thermal expansion (free elongation of the TGO) is assumed to be dependent on temperature and therefore is expressed in Equation (5).

$$\frac{\Delta L(T)}{L} = a_0\left(T - T_{sf}\right) + \frac{1}{2}a_1[(T-T_{amb})^2 - \left(T_{sf} - T_{amb}\right)^2] \qquad \textbf{(5)}$$

where T is EB-PVD/metal ceramic interface temperature, T_{sf} is the strain (or stress) free temperature for the oxide, T_{amb} is ambient temperature and α_0 and α_1 are the thermal expansion coefficients.

The damage term is defined to be the inverse of N (i.e. N^{-1}) and the TBC is expected to fail when the accumulated damage reaches one (1). The damage component D_i is defined by Equations (6) and (7).

$$D_i = \frac{1}{N} = \left[\left(\frac{\Delta\varepsilon_{ff}}{\Delta\epsilon}\right)\left(1 - \frac{\delta}{\delta_C}\right)^C + \left(\frac{\delta}{\delta_C}\right)^C\right]^{-b} \quad \textbf{(6)}$$

$$\mathrm{D} = \sum_i D_i < 1 \quad \textbf{(7)}$$

Blade Creep Life Assessment

To predict and analyze the influence of TBC oxidation on gas turbine creep life, it was imperative to develop a creep life assessment model. Therefore, a physics-based creep life assessment model was developed based on the earlier work done at Cranfield University [9, 19] and applied to the HPT first stage rotor blade. The creep life assessment model was based on a 2D analytical approach consisting of three main sub models which include stress, thermal and life estimation models.

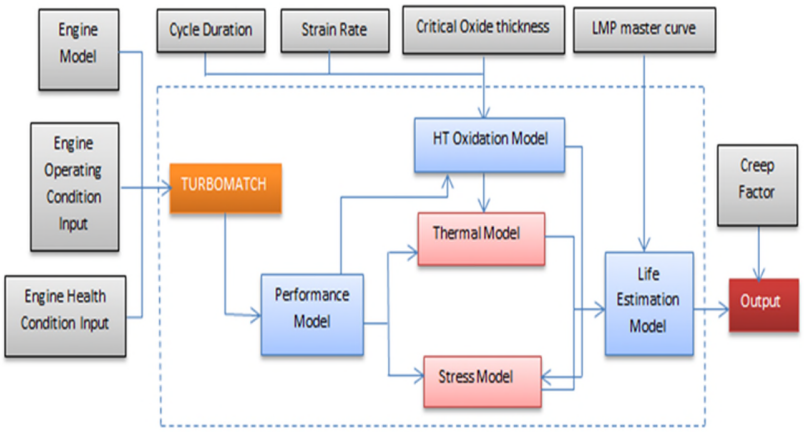

Figure 1: Integrated Creep Life Assessment Model

The stress model calculates the maximum stress acting on the blade whereas the thermal model estimates the blade metal temperature. The creep life estimation model evaluates the creep life of the blades and displays the results as a Creep Factor. Figure 1 shows the methodology used for the research.

Stress Model

The stress model calculates the total stress acting on the blades. Two main sources of stress have been considered in this study: stresses due to centrifugal load caused by engine rotation and stresses due to gas bending momentum.

The thermodynamic data such as rotational speed, gas temperature and pressures were calculated by TURBOMATCH. For simplicity, it is assumed that the axial velocity along the blade span is constant and the

forces (centrifugal loading, static pressure difference and momentum change) act on the center of gravity of blade sections.

The variations of the blade stresses are predicted at locations along the blade span and chord. At span-wise, the blade span was divided into sections at intervals of 25% of the span whereas the chord was split into three areas namely blade leading edge (LE), trailing edge (TE) and the back of the blade as depicted in Figures 3 and 5. The centrifugal force for each section of the blade (Figure 2) is calculated using Equation (8) [20].

$$F_{sec} = \rho \times A_{CsAv} \times H_{sec} \times w^2 \times r_{cg} \quad \textbf{(8)}$$

where ρ is the material density, A_{CsAv} is the average cross sectional area between the top and bottom sections, h_{sec} is the blade section height, w is the angular speed, r_{cg} is the distance between the rotation axis and the section centre of gravity. The calculated F_{sec} was used to calculate the centrifugal stress using Equation (9).

$$\sigma_{CFsec} = \frac{\sum F_{sec}}{A_{cs}} \quad \textbf{(9)}$$

where A_{cs} is the cross sectional area of the corresponding section.

The pressure force of each blade section (PF_{Sec}) is calculated using Equation (10) [20] and consequently the blade bending moment due to the static pressure is calculated using Equation (11) [20].

$$PF_{sec} = \frac{A_{AnSec} \times \Delta\rho_{AvSec}}{N_b} \quad \textbf{(10)}$$

$$BMP_{sec} = \sum (PF_{sec} \times d_{CGsec}) \quad \textbf{(11)}$$

where A_{Ansec} is the blade section annulus area, $\Delta\rho_{Avsec}$ is the average section static pressure difference, N_b is the number of blades, and d_{CGsec} is the distance between the section centers of gravity to the respective sections.

The gas velocity change across the blade (inlet and outlet) causes a momentum change of the gas along the axial and tangential directions. Therefore, the blade section momentum forces for both the axial and tangential directions, VF_{sec} are computed using Equations (12) and (13) [20] .

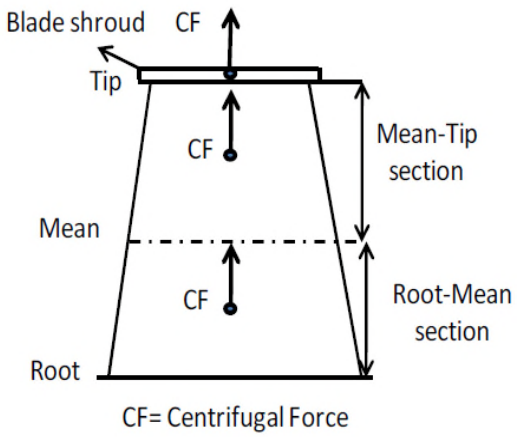

Figure 2: Blade centrifugal forces

$$VF_{Axsec} = \frac{m_{Area} \times A_{AnSec} \times \Delta V_{AxSec}}{Nb} \quad \textbf{(12)}$$

$$VF_{Tansec} = \frac{m_{Area} \times A_{AnSec} \times \Delta V_{TanSec}}{Nb} \quad \textbf{(13)}$$

where m_{Area} is the mass flow per unit area of the section annulus, ΔV_{AxSec} and ΔV_{TanSec} are axial and tangential velocity difference respectively.

The blade bending moments due to the axial and tangential forces at each blade section BMV_{AXsec} and BMV_{Tansec} are calculated using Equations (14) and (15) [20].

$$BMV_{Axsec} = \sum (VF_{AxSec} \times d_{CGsec}) \quad \textbf{(14)}$$

$$BMV_{Tansec} = \sum (VF_{TanSec} \times d_{CGsec}) \quad \textbf{(15)}$$

Subsequently, Equations (16) and (17) [20] are used to compute the resulting bending moment at the blade direction (about *X* and *Y* axis).

$$M_{xx} = (BMP_{sec} + BMV_{AxSec})sin\theta + BMV_{TanSec}cos\theta \quad \textbf{(16)}$$

$$M_{yy} = (BMP_{sec} + BMV_{AxSec})cos\theta - BMV_{TanSec}sin\theta \quad \textbf{(17)}$$

where θ is the blade stagger angle, M_{xx} and M_{yy} are the blade section resulting bending moments about *x* and *y* axes, M_{xx} and M_{yy} are in turn used to calculate the bending moment at the three different locations along the blade chord (LE, TE and back of the blade) using Equation (18) [20].

$$\sigma_{BMsec} = \frac{M_{xx}}{I_{min}} Y + \frac{M_{yy}}{I_{max}} X \quad \textbf{(18)}$$

where *X* and *Y* are the distances from the *LE*, *TE* and the back of the blade from the *XX* and *YY* axes as depicted in Figure 3, I_{max} and I_{min} are the maximum and minimum values of the blade section moments of inertia.

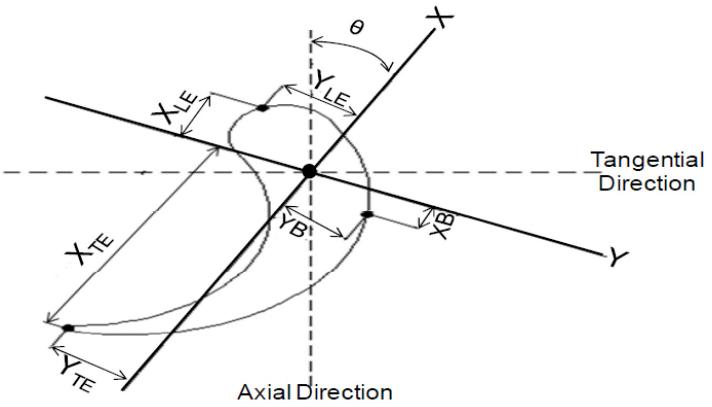

Figure 3: Schematic diagram of the blade and gas directions [20]

The maximum stress at each of the blade sections (centrifugal loading and gas bending moment) is calculated using Equation (19).

$$\sigma_{TotSec} = \sigma_{CFsec} + \sigma_{BMsec} \quad \textbf{(19)}$$

The blade geometry and operating condition will determine the location of the blade section where the maximum stress will occur. It could be either the LE, TE or back of the blade.

Thermal Model

The thermal model was developed and used to estimate the blade temperature. The blade is regarded as a heat exchanger which is subjected to a mainstream of hot gas flow from the burner. The main elements of the model are the cooling methods, the blade geometry, the TBC thickness, the heat transfer coefficients, the gas properties, the Radial Temperature Distribution Factor (RTDF), the blade material etc. The temperature profile through the blade with TBC and film cooling is presented in Figure 4.

Similar to the stress model, the thermal model uses a 2-dimensional approach that evaluates the temperature variation at each blade section. By specifying a value of RTDF which should not be more than 0.2 [21], the maximum gas temperature (T_{max}) and minimum gas temperature (T_{min}) are calculated using Equations (20) and (21) [21].

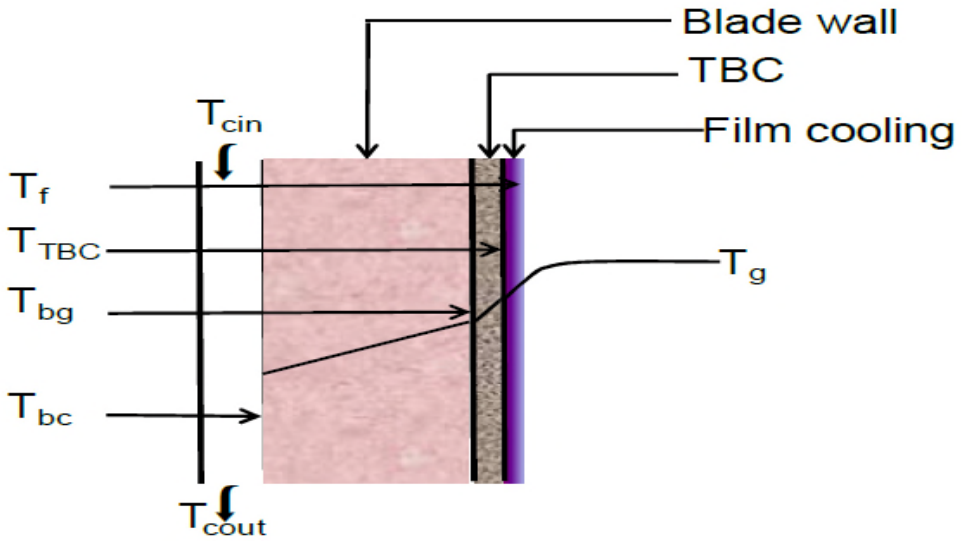

Figure 4: **Temperature profile of a blade with TBC and film cooling** [19]

RTDF depicted in Figure 5, is the ratio of the difference between the circumferentially peak gas temperature (T_{max}) and the gas mean temperature (T_{mean}) to the combustor temperature rise (T_{ref}), Equation (22).

$$T_{max} = T_{OIN} + (T_{REF} \times RTDF) \quad \textbf{(20)}$$

$$T_{min} = \frac{(5T_{OIN} - 2T_{max})}{3} \quad \textbf{(21)}$$

$$\text{RTDF} = \frac{T_{max} - T_{mean}}{T_{ref}} \quad \textbf{(22)}$$

where T_{OIN} is the rotor inlet temperature and T_{ref} is temperature rise of the burner. It is assumed that the maximum temperature along the blade span occurs at around 75% distance from the blade root as shown in Figure 5. Furthermore, the following assumptions were used in the course of building the thermal model:

- The gas temperature rise from the root to 75% distance from the root is linear.
- Similarly, the reduction in gas temperature from 75% to the tip of the blade is also linear.
- The minimum gas temperature occurs at the root and tip of the blade.

The rotor inlet gas temperature T_{OIN} is evaluated by considering the mixing effect between the coolant flow exiting the NGV and the core flow as depicted in Equation (23).

$$T_{OIN} = \frac{m_g Cp_h T_{OIN(Bef)} + m_{cNGV} CP_c T_{CoNGV}}{(m_g + m_{cNGV}) Cp_h} \quad \textbf{(23)}$$

where m_g is gas mass flow rate, Cp_h and Cp_c are specific heats of the hot and the cold gas flow respectively, m_{cNGV} is the NGV coolant mass flow rate and T_{coNGV} is the NGV coolant exit temperature. $T_{OIN(Bef)}$ and T_{coNGV} in Equation (23) are calculated using Equations (24) and (25) respectively.

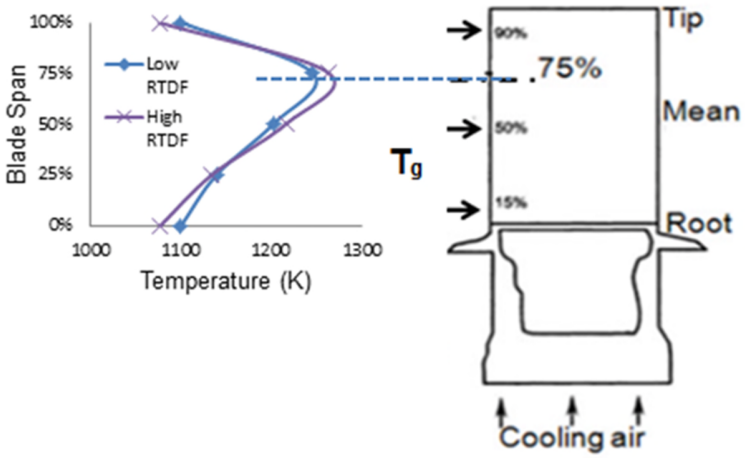

Figure 5: **Average radial temperature distribution profile at the inlet of a turbine rotor blade** [19]

$$T_{OIN(Bef)} = \mathrm{TET} - \frac{m_{cNGV} CP_c}{m_g CP_h} (T_{C0NGV} - T_{ciNGV}) \quad \textbf{(24)}$$

$$T_{coNGV} = T_{ciNGV} + \eta_{conNGV}(T_{NGV} - T_{ciNGV}) \quad \textbf{(25)}$$

where *TET* is the turbine entry temperature, T_{ciNGV} is the *NGV* inlet coolant temperature, η_{conNGV} is the *NGV's* convention efficiency and T_{NGV} is the *NGV* metal temperature. In order to predict the rotor blade metal temperature, the coolant inlet temperature for the rotor blade section is taken from the exit temperature of the previous section from root to top. The rotor blade section metal temperature is calculated using Equation (26) [22].

$$T_{MSec} = T_{Gsec} - \varepsilon(T_{Gsec} - T_{cisec}) \quad \textbf{(26)}$$

where T_{Gsec} is the section gas temperature, T_{cisec} is the section coolant temperature and ε is the rotor cooling effectiveness which is calculated using Equation (27) [23] and the calculated cooling effectiveness is applicable for all the blade sections.

$$\varepsilon = \frac{(1 + Bi)m * \eta_c + \varepsilon_f(1 - \eta_c)}{1 + (1 + Bi)m * \eta_c - \varepsilon_f\eta_c} \quad \textbf{(27)}$$

where, *Bi* is the Biot number, *m** is mass flow function, η_c is internal convection efficiency, ε_f is the film cooling effectiveness. Biot number is calculated using Equation (28) [23].

$$\mathrm{Bi} = h_g \frac{\Delta x}{k_{TBC}} \quad \textbf{(28)}$$

where h_g is the heat transfer coefficient, Δx is the *TBC* thickness and k_{TBC} is the *TBC* ceramic conductivity. Heat transfer coefficient is calculated using Equation (29).

$$h_g = \frac{Nu_g k}{d_{sec}} \quad \textbf{(29)}$$

where Nu_g is the Nusselt number, k is conductivity and d_{sec} is the section blade chord.

Life Estimation Model

The Larson Miller Parameter (LMP) [24] is used to evaluate the creep life. From Arrhenius's Law, the LMP equation can be expressed by Equation (30):

$$\mathrm{P} = 10^{-3} T_M \left(log t_f + C \right) \quad \textbf{(30)}$$

Therefore, time to fracture (t_f) can be expressed with Equation (31):

$$t_f = 10^{\left(\frac{1000P}{T_M}\right) - C} \quad \textbf{(31)}$$

where T_M is the blade material temperature; P is the LMP while C is the parameter constant. Generally the value of C is chosen between 17 and 23 while for industrial gas turbines, it is generalized as 20.

Once the rotor blade stress and metal temperature are predicted using the stress and thermal models respectively, the time to fracture of the rotor blade can be estimated using the creep life estimation model shown by Equations (30) and (31). The creep life at different sections of the rotor blade may be different as stresses and metal temperatures vary at different sections of the blade. Therefore, the creep life is expected to vary in different sections.

Creep Factor

Creep Factor (*CF*), a concept which was developed by Abdul Ghafir et al. [9] is defined as the ratio between the actual creep life and the creep life at a reference condition. The *CF* approach is adopted for this research to quantify the impact of actual operating conditions on creep life of gas turbine engines because it appraises the rate of creep life consumption relative to a specific operating condition desired by the operator. The *CF* is denoted as:

$$\mathrm{CF} = \frac{L_C}{L_{cRef}} \tag{32}$$

where L_c denotes the remnant life for engine operated at actual operating condition and L_{cRef} represents the reference remnant life at an user-defined reference operating condition. In general:

- *CF=1* means that the engine has the same creep life as that of the engine at the reference operating condition, i.e. $L_c = L_{cRef}$.
- *CF>1* represents a situation where the engine consumes creep life slower or has longer creep life compared to that of the engine operating at the reference operating condition.
- *CF<1* represents a situation where the engine consumes creep life more quickly or has shorter creep life compared with that of the engine operating at the reference condition.

APPLICATION

Engine Performance Simulation and Blade Geometry

In order to study the impact of TBC oxidation on gas turbine engine creep life, a model aero derivative gas turbine engine similar to GE LM2500+ was created in this study based on the engine performance specification [25] listed in Table 1.

Table 1: Engine Performance Parameters [25]**.**

Parameter	Value	Unit
Pressure ratio	23.1	
Exhaust gas flow rate	82.5	Kg/s
Power Output	28.85	MW
Thermal Efficiency	39	%

TURBOMATCH [10], gas turbine engine performance simulation and diagnostics software developed at Cranfield University, was used to create a performance model based on the engine configuration shown in Figure 6 where it has an axial compressor driven by a compressor turbine, a combustor and a power turbine providing power output.

The performance simulations provided essential performance information of the thermodynamic cycle of the model engine under investigation. Using the results from the performance simulations and available information from open literature, the blades of the first stage of the HP turbine of the model engine were sized using the constant mean diameter method [26-27]. The model blade geometry at the mid-height as obtained from the blade sizing model are presented in Table 2

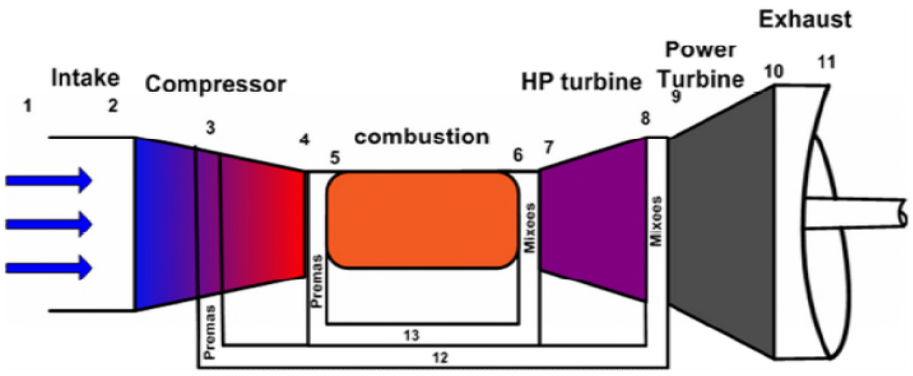

Figure 6: Layout of 2-shaft aero-derivative engine.

Table 2: Parameters at blade mid height

Parameter	**Value**	**Unit**
Spacing	0.0234	M
Optimum axial solidity	1.00	
Axial chord	0.0234	M
Axial aspect ratio	1.4	
Stagger angle	35	Degrees

Results from the blade sizing model were used to obtain the blade shape. Cooling passages are introduced to depict a cooled blade in order to reduce blade metal temperature using the air extracted from the compressor. For simplicity, only four internal cooling passages are introduced in the model blades. Other important turbine blade data such as blade materials, cooling effectiveness, size of leading and trailing edges, cross sectional areas, blade speed, etc. were specified but their values are not stated here for simplicity.

Effect of TET & PCN on TBC Life

The effect of mechanical strain on the oxidation behavior of TBCs of the HP turbine blades at different TETs was studied and the results are illustrated in Figure 7 where strain is represented as a relative value to a baseline strain. The TBC life is reduced substantially as the strain increases from the baseline and also reduced as TET increases. For instance, at a TET of 1505K, a 15% increase in strain reduces the TBC life by 45%. This means that the strain on the substrate material, which is caused either as a result of TET or PCN increase, has a significant influence on TBC life as illustrated in Figure 8.

This is because an increase in engine rotational speed (PCN) increases the mechanical stress which directly increases the total maximum stress acting on the blade and the coatings. Given that stress is directly proportional to the strain, an increase in the stress increases the strain on the blade and the coatings. This results in shear stress development on the coatings and the loss of TBC life.

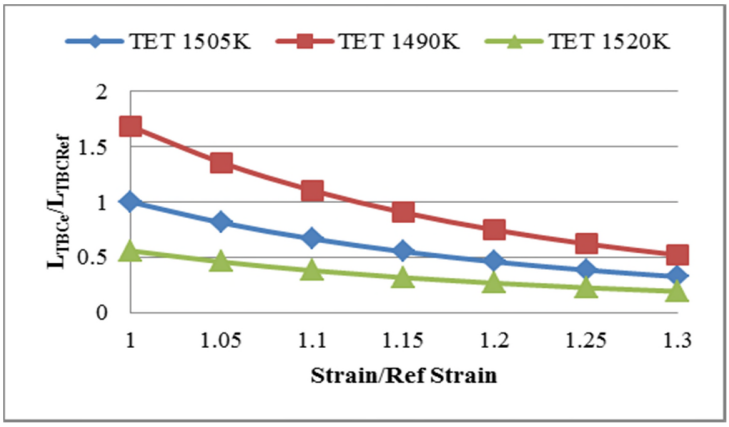

Figure 7: Strain effects on TBC life at different TBCs.

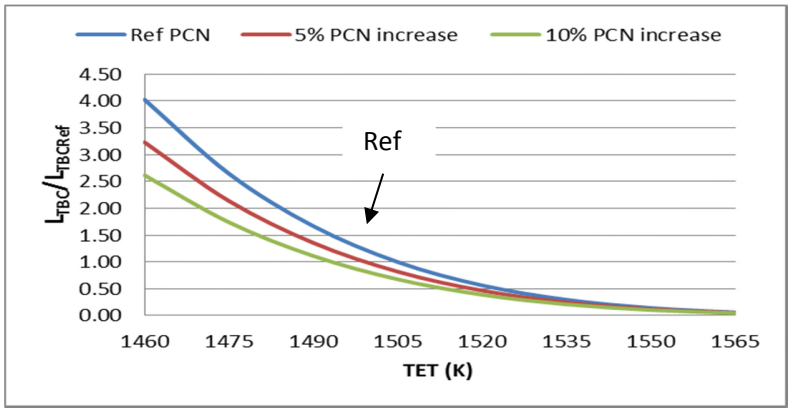

Figure 8: Effect of TET on TBC life at different PCN.

Similarly, for a strain/ref strain of 1.05, as TET increases from 1505K to 1520K, the TBC life is reduced by 44%; it is therefore evident that the increase of firing temperatures (TET) to improve the engine's power and efficiency has a detrimental effect on the TBC life. In this case, the effects on TBC are intensified by the presence of oxidation damage. This is because the bond coat which has the responsibility of mitigating the effect of thermal expansion mismatch stresses, oxidizes significantly at high temperatures. As the bond coat oxidizes, the residual stresses in addition to the increase in Coefficient of Thermal Expansion (CTE) as well as the thermal stresses imposed by cycling effect results in the formation of cracks on the surface of the bond coat which causes spallation. This is in agreement with the findings of Wright KP [28].

Effect of Ambient Temperature on TBC Life

The ambient temperature also plays a vital role in determining the oxidation failure of TBCs. By using the integrated model, the impact of ambient temperature variation on the TBC failure due to oxidation was

studied for different strain levels. The results obtained are presented in Figure 9 which shows that TBC life gradually decreases with an increase in ambient temperature. It is worth noting that the rate of decline in TBC life is relatively stable when the ambient temperature is lower than 15^0C and becomes more significant when the ambient temperature is higher than 15^0C.

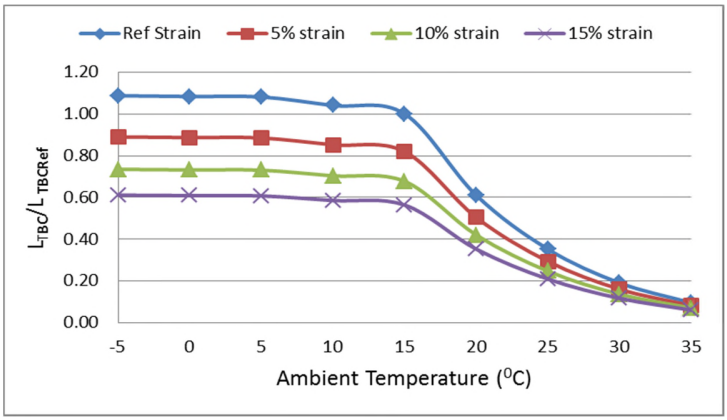

Figure 9: Ambient temperature effects on TBC life at different strain.

It can be argued that at low ambient temperatures (below 15^0C), the TBC oxidation is affected mainly by the mechanical strain and not much by the thermal strain. There is a sharp decrease in the TBC life when ambient temperature is higher than 15^0C, which shows that at higher ambient temperature, the temperature effect plays a significant role in the oxidation behavior of TBCs and in fact becomes a more dominant factor than the strain effect. This is due to the fact that as the ambient temperature increases, the air becomes hotter and more difficult to be compressed in the compressor. Therefore the compressor turbine will be required to produce more work to drive the compressor. In doing this, the turbine entry temperature is raised and this will cause the bond coat to oxidize at a faster rate. Hence, the thermal load effect on TBC becomes the determinant factor.

Impact of TBC Failure on Blade Metal Temperature

The failure of TBCs due to oxidation will result in the exposure of the substrate materials to very high temperatures. Therefore, the blade temperature variation along the span of the HPT blade before and after TBC failure was examined. The results are illustrated in Figure 10 and Figure 11.

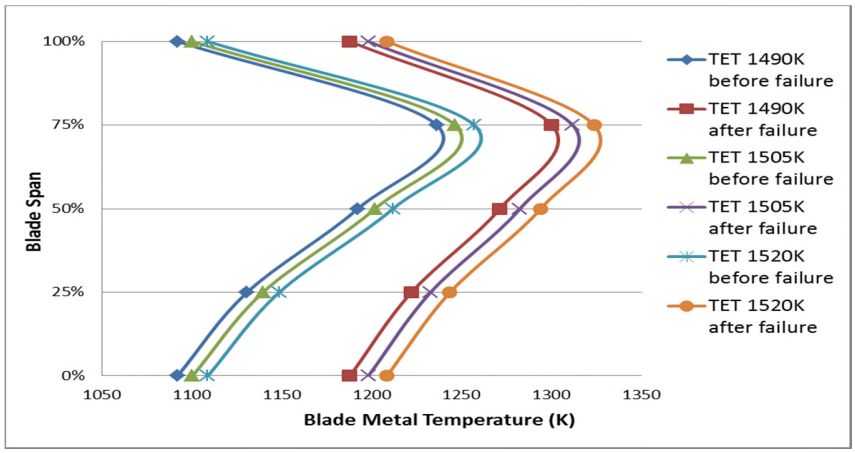

Figure 10: Effect of TBC failure on blade temperature.

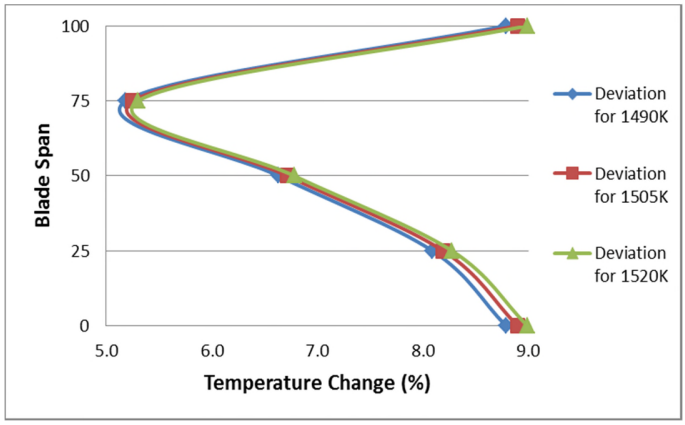

Figure 11: Blade metal temperature deviation due to different TETs.

The impact of three different TETs (1490K, 1505K and 1520K) on blade metal temperature was considered. It can be seen in Figure 10 andFigure 11 that the blade metal temperature would be increased by between 120^0C (at the blade root and tip) and 75^0C (at the 75% mark from the blade root), or increased by between 9% and 5.2%.

Effect of TBC Oxidation Failure on Blade Creep Life

The integrated creep life model was used to assess the impact of TBC oxidation on the HPT blade creep life. This was demonstrated by considering TBC oxidation on blade creep life at different TETs and strain levels and the impact of ambient temperature on the blade creep life due to TBC oxidation failure.

The results of the impact of TBC oxidation on the blade creep life are illustrated in Figure 12 and they show that the TBC oxidation has a significant effect on blade creep life. For instance, at a TET/T_{ref} value of 0.98 and for the reference strain, the creep life of the blade could be reduced by about 14% when compared with that without the effect of TBC oxidation. A further increase of 5% in the strain from the reference value could reduce the creep life by 31%. Again at high firing temperatures, the TET variation dominates the creep behavior because of the fast oxidizing rate of the bond coats while the effect of mechanical strain becomes less significant as the Creep Factors for different strains approach to a single value. On the other hand at low TET, both the strain and the temperature variations affect the creep behavior of the blades.

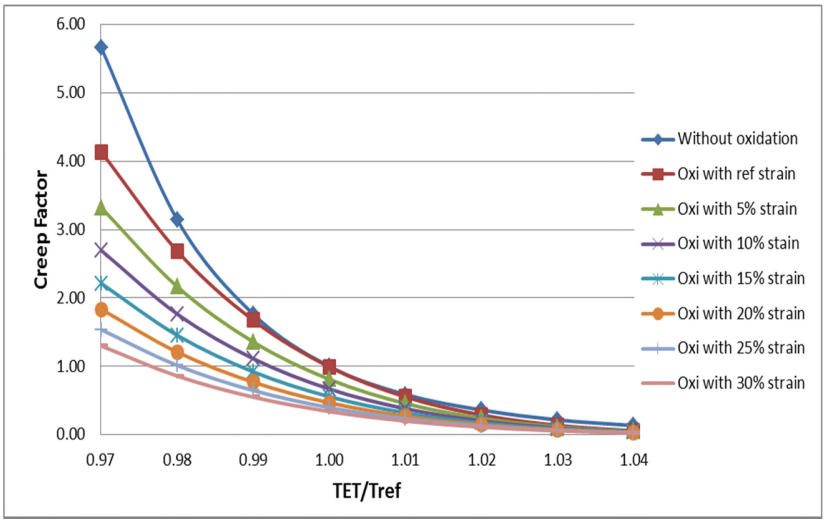

Figure 12: TBC oxidation on blade creep life at different TETs and strain levels.

To investigate the effect of ambient temperature on the creep life of the model aero-derivative gas turbine it was assumed that the cycle duration is 12 hours and the average ambient temperature changes every 2 hours. Therefore, ambient temperature profiles on a typical day in four seasons were assumed and shown in Figure 13.

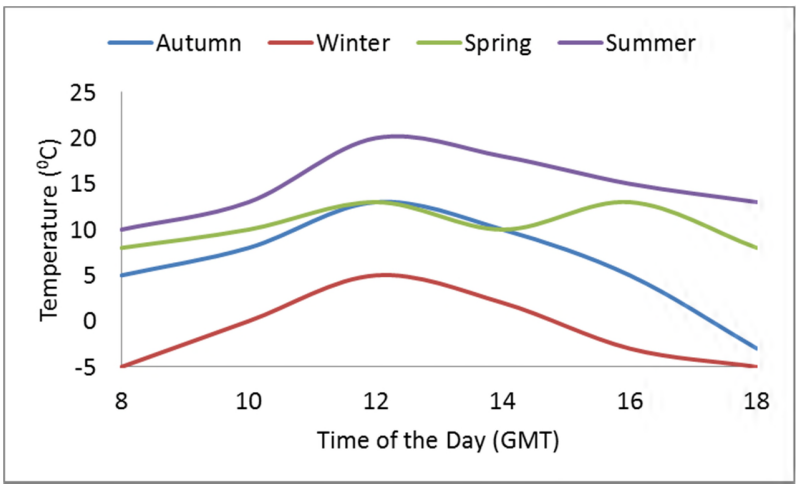

Figure 13: Day temperature profile.

The engine shaft power was kept constant irrespective of the changing ambient condition. The ambient temperature variations and their impact on the critical performance parameters of the engine, such as PCN and TET are illustrated in Figure 14 and Figure 15.

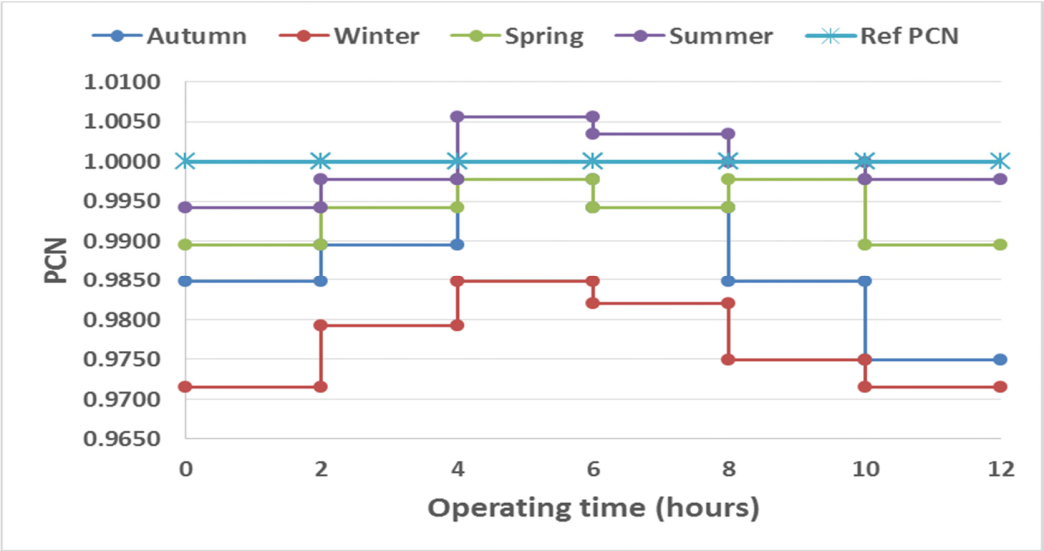

Figure 14: PCN variation for different ambient conditions at constant power.

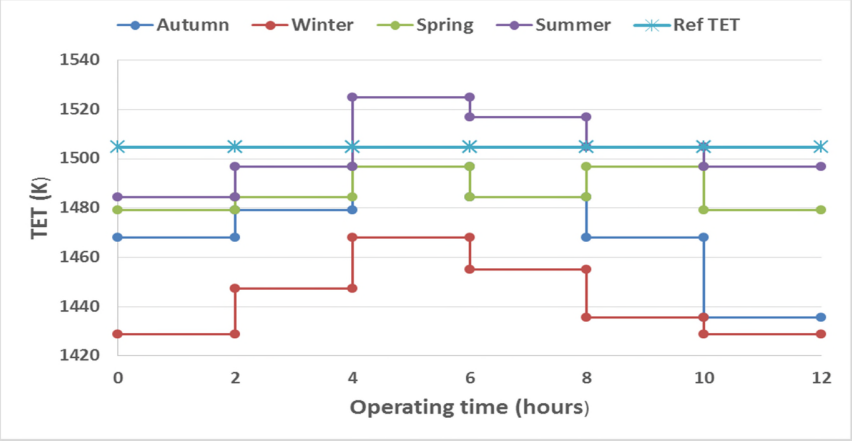

Figure 15: TET variation for different ambient temperature at constant power.

With the consideration of the changing daily ambient temperatures, the Creep Factor approach was used to assess the impact of the TBC oxidation on the creep life of the HPT blades for the different seasons of the year. The results are presented in Figure 16 and Figure 17 showing that TBC oxidation reduces the creep life of the HPT blade in two extreme weathers.

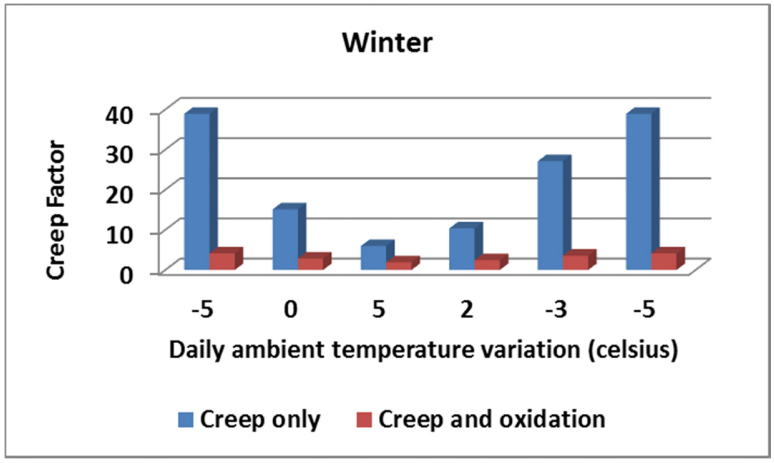

Figure 16: Creep variation during winter.

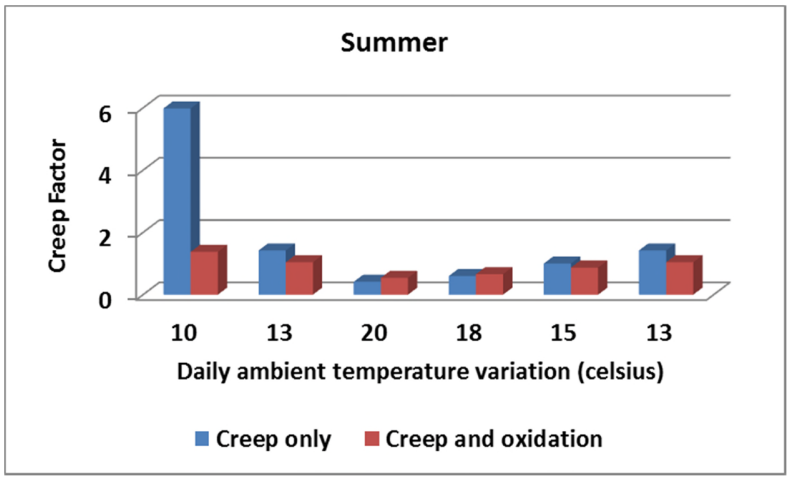

Figure 17: Creep variation during summer.

Based on the above results, the average Creep Factor for the four seasons using Equation (32) are shown in Figure 18. It can be seen that the highest impact was observed in winter (December, January and February) while the least impact was in summer (June, July and August).

The impact of the TBC oxidation on the life usage for the different seasons was examined. The life usage represents the percentage of the blade creep life that has already been consumed relative to the total life of the blade. The results are illustrated in Figure 19, which demonstrates that the TBC oxidation increases the life usage of the engine for all the conditions considered. It can be seen from Figure 19 that the life usage for autumn increases from 0.64% to 1.32% when TBC oxidation effect is considered. Similarly in winter, the life usage increased from 0.15% to 0.73% whereas in spring and summer, the life usage increased from 1.02% to 2.6% and 2.42% to 2.60% respectively when TBC oxidation effects are considered. Consequently, TBC oxidation increases the overall life usage of the gas turbine engine from 4.22% to 6.35% for one calendar year.

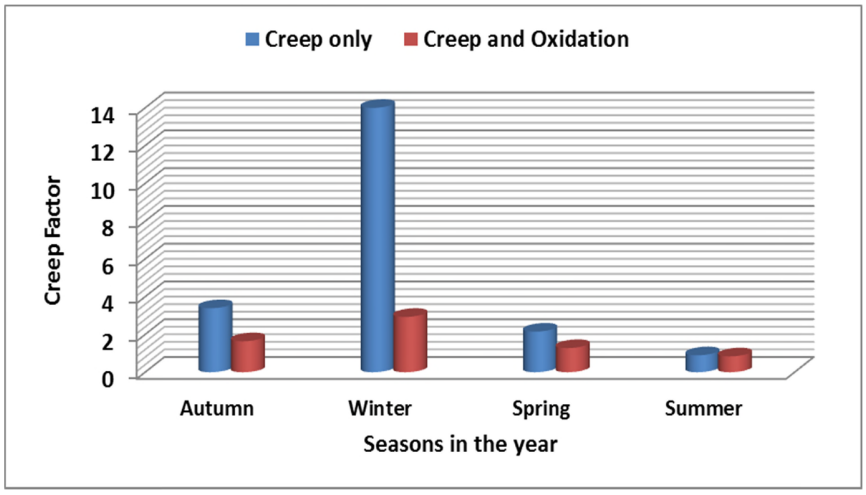

Figure 18: Creep and oxidation effects**.**

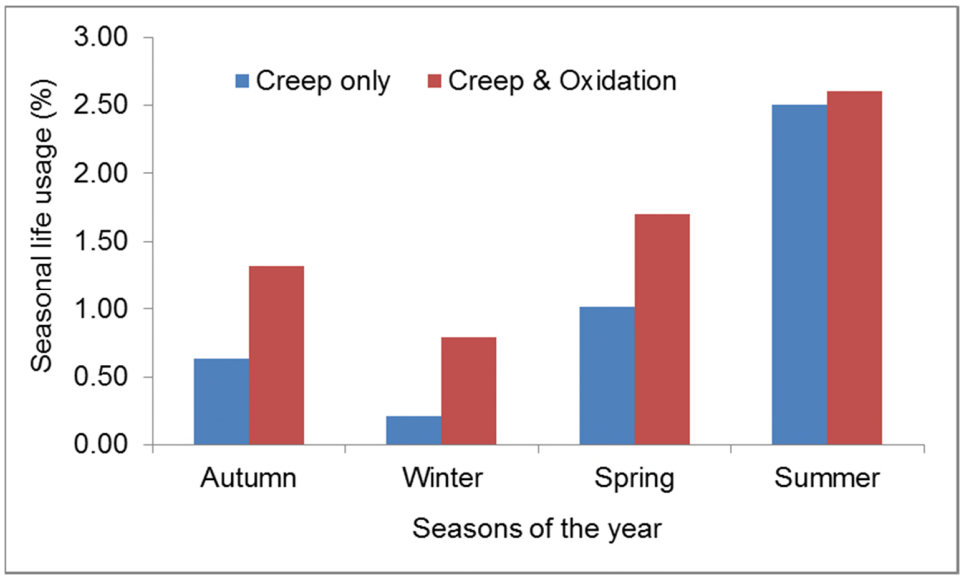

Figure 19: Impact of TBC oxidation on the overall life usage.

CONCLUSIONS

This paper presents a novel creep life analysis model for gas turbine engines with the consideration of the impact of TBC oxidation on the HPT blade life. The integrated creep life analysis model comprises of stress,

thermal, oxidation and creep life estimation models. It has been used to assess the impact of TBC oxidation on the creep life of the HPT blades, the critical creep life limiting components of a model aero derivative gas turbine engine in two test cases. The results show that the TBC oxidation has a significant detrimental effect on the creep life of the turbine blades. For example, the creep life of the blade was reduced by about 14% when compared with that without the effect of the TBC oxidation. The TBC oxidation increases the cumulative life usage of the model gas turbine during autumn from 0.64% to 1.32%. Similarly, the engine life usage could be increased from 0.15% to 0.73% in winter, from 1.02% to 2.6% in spring and from 2.42% to 2.60% in summer respectively.

NOMENCLATURE

ΔH = Change in enthalpy

Δp_{Avsec} = Average section static pressure difference.

Δx = TBC thickness.

$\Delta \epsilon$ = TGO inelastic strain range

$\Delta \epsilon_{ff}$ = Mechanical inelastic strain range

A = Empirical Constant

A_{Ansec} = Blade section annulus area.

A_{cs} = Cross sectional area of the corresponding section.

A_{CSAv} = Average cross sectional area between top and bottom section

B = Model constant.

Bi = Biot number

BMP_{sec} = Pressure bending moment at blade section.

BMV = Momentum bending moment at blade section.

C = Model constant.

C = Parameter constant.

CF = Creep Factor.

F_{sec} = Blade section centrifugal force

Cp_c = Specific heat of cold gas.

Cp_h = Specific heat of hot gas.

d_{CGsec} = Distance between the section's center of gravity to the respective section.

D_i = Damage component.

d_{sec} = Section blade chord.

h_g = Heat transfer coefficient.

H_{sec} = Blade section height.

I_{max}, I_{min} = Maximum and minimum moment of inertia.

ISA = International standard atmosphere.

K = Thermal conductivity.

k_{TBC} = TBC ceramic conductivity.

L_c = Remnant life for engine operated at actual operating condition.

L_{cRef} = Reference remnant life at a user-defined operating condition.

m = Empirical power law coefficient.

m^* = Mass flow function

m_{area} = mass flow per unit area.

m_{CNGV} = NGV coolant mass flow rate.

m_g = gas mass flow rate.

M_{xx}, M_{yy} = Blade section resulting bending moment about the X and Y axis.

N = constant.

N = Number of cycles.

N_b = Number of blades.

NGV = Nozzle guide vane.

Nu_g = Nusselt number.

P = Larson-Miller Parameter,

PCN = rotational speed.

PF_{sec} = Pressure force of each section.

Q = ΔH/R.

R = Universal gas constant.

r_{cg} = Distance between the rotation axis and the section centre of gravity.

$RTDF$ = Radial temperature distribution factor.

T = Gas temperature.

T = time.

T_0 = Temperature at a reference condition.

T_{amb} = Ambient temperature.

T_{bc} = Blade coolant temperature.

T_{bg} = Blade metal temperature.

TC = Top coat.

T_{Cin} = Inlet coolant temperature.

T_{cinNGV} = NGV inlet coolant temperature.

T_{CiSec} = Section Coolant temperature.

T_{coNGV} = NGV coolant exit temperature.

T_{cout} = Outlet coolant temperature.

TET = Turbine entry temperature.

T_f = Film coolant temperature.

t_f = time to fracture.

T_g = Gas temperature.

T_{Gsec} = Section gas temperature.

T_M = Material temperature.

T_{max} = Maximum gas temperature.

T_{mean} = Gas mean temperature.

T_{min} = Minimum gas temperature.

T_{MSec} = Section's blade metal temperature.

T_{NGV} = NGV inlet coolant temperature.

T_{OIN} = Rotor inlet temperature.

T_{ref} = Burner temperature rise.

T_{sf} = Strain or stress free temperature.

T_{TBC} = TBC temperature.

VF_{Axsec} = Axial blade section momentum force.

VF_{Tansec} = Tangential blade section momentum force.

W = Angular speed.

X, Y = Distance between the corresponding location to the blade's section center of gravity.

α_0 = Thermal expansion coefficient.

α_1 = Thermal expansion coefficient.

δ = TGO thickness in microns.

δ_c = Critical oxide thickness.

ϵ = TGO strain.

ε = Overall cooling efficiency.

ε = Mechanical strain.

ε_f = Film cooling efficiency.

ϵ_{ss} = Substrate total strain.

η_c = Internal convection efficiency.

η_{conNGV} = NGV convection efficiency.

θ = Blade stagger angle.

ρ = Density.

σ_{BMSec} = Section's bending moment stress.

σ_{CFSec} = Centrifugal stress at each blade section.

σ_{TotSec} = Total maximum stress at each blade section.

ACKNOWLEDGMENTS

This research has been funded by the Bayelsa State Government of Nigeria, the support of which is gratefully acknowledged.

REFERENCES

[1] Schlachter, W. and Gessinger, G. (1990), "Innovation in Power Engineering - Role of Materials", *High Temperature Materials for Power Engineering,* 24-27 September, Liege, Belgium, Kluwer Academic Publishers.

[2] Kilgallon, P., Simms, N. J. and Oakey, J. E. (2002), in Lecomte-Beckers (ed.), *Materials for Advanced Power Engineering,* Forschungzentrum, pp. 903.

[3] Allen, D. H., Oakey, J. E. and Scarlin, B. (1998), in Lecomte-Beckers (ed.), *Materials for Advanced Power Engineering,* pp. 1825.

[4] Jansohn, P. (2013), *Modern gas turbine systems: High efficiency, low emission, fuel flexible power generation,* Elsevier.

[5] Miller, R. A. (1997), "Thermal barrier coatings for aircraft engines: history and directions", *Journal of Thermal Spray Technology,* vol. 6, no. 1, pp. 35-42.

[6] Roy, N., Ghosh, R. N. and Pandey, M. C. (2001), "Modelling of Interaction between Creep and Oxidation behavior for Engineering Materials", *ISIJ International,* vol. 41, no. 8, pp. 915-921.

[7] Eriksson, R., Brodin, H., Johansson, S., Östergren, L. and Li, X. (2011), "Influence of isothermal and cyclic heat treatments on the adhesion of plasma sprayed thermal barrier coatings", *Surface and Coatings Technology,* vol. 205, no. 23, pp. 5422-5429.

[8] Chen, L. (2006), "Yttria-stabilized zirconia thermal barrier coatings—a review", *Surface Review and Letters,* vol. 13, no. 05, pp. 535-544.

[9] Ghafir, M. A., Li, Y., Singh, R., Huang, K. and Feng, X. (2010), "Impact of Operating and Health Conditions on Aero Gas Turbine: Hot Section Creep Life Using a Creep Factor Approach", *ASME Turbo Expo 2010: Power for Land, Sea, and Air,* American Society of Mechanical Engineers, pp. 533.

[10] MacMillan, W. L. (1974), *Development of a modular-type computer program for the calculation of gas turbine off-design performance,* , Cranfield Institute of Technology.

[11] Meier, S., Nissley, D., Sheffler, K., and Cruse TA, (1992), "Thermal Barrier Coating Life Prediction Model Development", *TRANSACTIONS-AMERICAN SOCIETY OF MECHANICAL ENGINEERS JOURNAL OF TURBOMACHINERY,* vol. 114, no. 2, pp. 258-263.

[12] Miller, R. A. and Lowell, C. E. (1982), "Failure mechanisms of thermal barrier coatings exposed to elevated temperatures", *Thin Solid Films,* vol. 95, no. 3, pp. 265-273.

[13] Berndt, C. C. and Herman, H. (1983), "Failure during thermal cycling of plasma-sprayed thermal barrier coatings", *Thin Solid Films,* vol. 108, no. 4, pp. 427-437.

[14] Tsai, H. and Tsai, P. (1995), "Microstructures and Properties of Laser-Glazed Plasma-Sprayed ZrO2-YO1. 5/Ni-22Cr-10Al-1Y Thermal Barrier Coatings", *Journal of materials engineering and performance,* vol. 4, no. 6, pp. 689-696.

[15] Kuroda, S. and Clyne, T. (1991), "The quenching stress in thermally sprayed coatings", *Thin Solid Films,* vol. 200, no. 1, pp. 49-66.

[16] Lee, J., Ra, H., Hong, K. and Hur, S. (1992), "Analysis of deposition phenomena and residual stress in plasma spray coatings", *Surface and Coatings Technology,* vol. 56, no. 1, pp. 27-37.

[17] Martena, M., Botto, D., Fino, P., Sabbadini, S., Gola, M. and Badini, C. (2006), "Modelling of TBC system failure: Stress distribution as a function of

TGO thickness and thermal expansion mismatch", *Engineering Failure Analysis,* vol. 13, no. 3, pp. 409-426.

[18] Busso, E., Lin, J., Sakurai, S. and Nakayama, M. (2001), "A mechanistic study of oxidation-induced degradation in a plasma-sprayed thermal barrier coating system.: Part I: model formulation", *Acta materialia,* vol. 49, no. 9, pp. 1515-1528.

[19] Eshati, S. (2011), *An evaluation of operation and creep life of stationary gas turbine engine* (unpublished PhD thesis), School of Engineering, Cranfield University, United Kingdom.

[20] Cookson and Haslam, A. (2011), *Mechanical Design of Turbomachinery* (unpublished Unpublisehed lecture note), Department of Power and Propulsion, School of Engineering, Cranfield University.

[21] Walsh, P. P. and Fletcher, P. (2004), *Gas turbine performance,* John Wiley & Sons.

[22] Horlock, J. and Torbidoni, L. (2006), "Turbine blade cooling: the blade temperature distribution", *Proceedings of the Institution of Mechanical Engineers, Part A: Journal of Power and Energy,* vol. 220, no. 4, pp. 343-353.

[23] Rubini. (2013), *Turbine Blade Cooling* (unpublished MSc Course Note), School of Engineering, University of Hull, United Kingdom.

[24] Larson, F. and Miller, J. (1952), "A time-temperature relationship for rupture and creep stresses", *Trans.ASME,* vol. 74, no. 5, pp. 765-775.

[25] Badeer, G. (2000), "GE aeroderivative gas turbines-design and operating features", *GER-3695E, GE Power Systems, Evendale, OH,*

[26] MacManus. (2012), *Turbomachinery Course Notes - Turbines* (unpublished MSc Course Note), School of Engineering, Cranfield University.

[27] Saravanamuttoo, H. I. H., Cohen, H., Rogers, G. F. C. and Straznicky, P. V. (2009), *Gas Turbine Theory,* Sixth ed, Pearson Prentice Hall, Harlow Essex England.

[28] Wright, P. and Evans, A. (1999), "Mechanisms governing the performance of thermal barrier coatings", *Current Opinion in Solid State and Materials Science,* vol. 4, no. 3, pp. 255-265.